Structure and Dynamics of Hydrated Ag (I): Ab Initio Quantum Mechanical-Molecular Mechanical Molecular Dynamics Simulation

Ria Armunanto,† Christian F. Schwenk, and Bernd M. Rode*

Department of Theoretical Chemistry Institute of General, Inorganic and Theoretical Chemistry University of Innsbruck, Innrain 52a, A-6020 Innsbruck, Austria

Received: December 19, 2002; In Final Form: February 21, 2003

A molecular dynamics simulation based on ab initio quantum mechanical forces in combination with molecular mechanics has been performed to describe structural and dynamical properties of Ag^+ in water. The first hydration shell, being the chemically most relevant region, was treated by quantum mechanics at Hartree−Fock level using the LANL2DZ ECP for Ag^+ and double-ζ plus polarization basis sets for water. The outer region of the system was described using a newly constructed classical three-body corrected potential derived from ab initio energy surfaces. The structure was evaluated in terms of radial and angular distribution functions and coordination number distributions. Water exchange processes between coordination shells have been investigated and evaluated. The results show that the first hydration shell is of rather irregular shape, with an average coordination number of 5.5. Fast water exchange processes between the first and second hydration shell were observed, leading to a preference of 5- and 6-fold coordinated species. The mean residence times of water molecules in the first and second hydration shell are 25 and 10 ps. Because of the labile structure, the librational and vibrational frequencies of first hydration shell ligands are only weakly influenced by the interaction with the ion.

1. Introduction

Structural and dynamical properties of metal ions in aqueous solution have become a major subject of experimental and theoretical investigations because of their important role in many processes in solution chemistry, biochemistry, and pharmacology. Ag^+−amino acid complexes which are soluble in water have biological and medical relevance, e.g., in antibacterial and antifungal activities.[1−4] Only few structural data have been obtained for hydrated Ag^+ from experimental work[5,6] and computer simulation study.[7]

Structural and dynamical properties of hydrated metal ions can be obtained both by experimental measurements and computer simulation methods. The main experimental methods are X-ray diffraction (XRD) and neutron diffraction (ND), extended X-ray absorption fine structure (EXAFS), and nuclear magnetic resonance (NMR).[5] Computer simulation methods as Monte Carlo (MC), classical molecular dynamics (CMD), and hybrid quantum mechanical and molecular mechanical (QM/MM) simulations have become a strong alternative to experiments for elucidating details of metal ion solvates, in particular for dilute systems and very fast exchange processes where experimental techniques reach their limitations. QM/MM simulations have been used successfully to simulate solvated metal ions in water or ammonia,[8−23] proving the need of this highly CPU time demanding method to obtain accurate data for such systems.[24]

In the first hydration shell of monovalent ions, the many-body interactions could be expected to be weaker than in the case of di- and trivalent ions, but the inclusion of three-body interactions to correct the pair potential function has generally been recognized as a significant improvement of the results.[18,25−32] To include higher *n*-body terms in the potential functions is a hardly feasible procedure, and thus, the QM/MM formalism providing the implicit inclusion of these many-body interactions at ab initio level for the most important region of the system is at present the most suitable procedure to reach this level of accuracy. To apply the quantum mechanical calculations to the full simulation box is still far for beyond current computer capacities. Therefore, only the chemically most relevant region of the system (QM region) is treated by ab initio quantum mechanics. In the case of hydrated ions, this is the first hydration shell, where many-body contributions are much more important than in the second shell or the bulk. The remaining region can be treated by molecular mechanics (MM region) based on pair potential functions, preferably still including three-body corrections.[9] The structure of the hydration shell of several metal ions has been successfully evaluated by QM/MM molecular dynamics simulation, and additionally hydration energies, librational, and vibrational spectra could be obtained.[5,16]

Ligand exchange processes at hydrated metal ions strongly influence ion reactivities. The rather labile structure of hydrated monovalent ions as Ag^+ compared to hydrated metal ions of higher charge makes their experimental investigation difficult. Experimental studies of hydrated Ag^+ have assigned 2−4.5 waters to the first hydration shell,[5,6] indicating that the shell structure is rather labile, subject to a rapid exchange between first and second shell ligands, and depending strongly on concentration and other experimental conditions.

As the lifetime of a ligand in the coordination shells of Ag^+ is extremely short, its detailed experimental analysis is almost impossible. On the other hand, QM/MM molecular dynamics simulations are most suitable to determine water exchange rates

* To whom correspondence should be addressed. E-mail: bernd.m.rode@uibk.ac.at.

† Permanent address: Austrian-Indonesian Center for Computer Chemistry, Chemistry Department, Faculty of Mathematics and Natural Sciences, Gadjah Mada University, Jogjakarta Indonesia.

10.1021/jp027769d CCC: $25.00
Published on Web 04/08/2003

TABLE 1: Optimized Parameters of the Analytical Pair Potential Function for the Interaction of Ag^+ with Water

pair	A (kcal mol^{-1} Å^6)	A (kcal mol^{-1} Å^8)	A (kcal mol^{-1} Å^9)	A (kcal mol^{-1} Å^{12})
Ag^+-O	−11187.36	130482.41	−175374.64	88248.29
Ag^+-H	−4341.34	73605.79	−118109.62	79786.24

in the picosecond range.[21] The labile hydrated Ag^+ thus appeared a most favorable example to use this capability of the QM/MM technique.

2. Methods

2.1. Potential Functions. To describe MM interactions between species in the system, two- and three-body interactions (Ag^+-H_2O and $H_2O-Ag^+-H_2O$) were included. More than 2000 ab initio energy points were fitted to an analytical two-body potential function

$$\Delta E^{2bd} = E^{ab}_{MW} - E^{ab}_{M} - E^{ab}_{W} \quad (1)$$

where ab denotes ab initio, MW denotes the ion−water, and M and W denote ion and water energies. The minimum energy for the Ag^+-H_2O interaction is −25.4 kcal mol^{-1} at a distance of 2.35 Å. MP2 calculations being much more time demanding[7] yield nearly the same Ag−O distance (3.32 Å) associated with a slightly lower energy (∼ −28.9 kcal/mol). As neither ion−ligand nor the shape of the potential curve are significantly different, it could be assumed that electron correlation would be neglected in the simulation, which otherwise would have consumed ∼30 instead of ∼7 months of CPU time. More than 9000 ab initio energy points were used to construct the three-body correction function, and the three-body energies (ΔE^{3bd}_{corr}) were computed as follows:

$$\Delta E^{3bd}_{corr} = (E^{ab}_{WMW} - E^{ab}_{M} - 2E^{ab}_{W}) - \Delta E^{2bd}_{MW}(r_1) - \Delta E^{2bd}_{MW}(r_2) - \Delta E^{2bd}_{WW}(r_3) \quad (2)$$

where ab and 2bd denote ab initio and pair potential energies; MW and WW indicate ion−water and water−water interactions, respectively; r_1, r_2, and r_3 correspond to ion−O(1), ion−O(2), and O(1)−O(2) distances. All pair and three-body interaction energies were calculated at the restricted Hartree−Fock (RHF) level with LANL2DZ ECP[33] and double-ζ plus polarization[34] basis sets for silver and water, respectively, and fitted to analytical functions using the Levenberg algorithm. The basis set superposition error (BSSE)[35] of our system was investigated and proved to be very small, amounting in 0.790 kcal/mol for an ion first shell water cluster. The water geometry was kept constant throughout the calculations, at experimental gas-phase values of O−H = 0.9601 Å and H−O−H = 104.47°.[36] Oxygen and hydrogen charges to be used in the function for Coulombic interactions were set to −0.6598 and 0.329937, respectively. All ab initio calculations were performed using the Turbomole[38−40] program.

The two-body ab initio energies were fitted to

$$\Delta E^{2bd}_{Fit} = \sum_{i=1}^{3} \frac{q_M q_i}{r_{Mi}} + \frac{A_i}{r_{Mi}^{6}} + \frac{B_i}{r_{Mi}^{8}} + \frac{C_i}{r_{Mi}^{9}} + \frac{D_i}{r_{Mi}^{12}} \quad (3)$$

where M and i denote Ag^+ and oxygen hydrogen atoms; A, B, C, and D are the optimized parameters; and q represent the atomic charges. The optimized parameters are summarized in Table 1.

The three-body correction energies were fitted to the equation

$$\Delta E^{3bd}_{Fit} = 0.37 e^{-0.31(r_1+r_2)} e^{-0.39 r_3} (CL - r_1)^2 (CL - r_2)^2 \quad (4)$$

where CL, set to 6.0 Å, is the cutoff limit beyond which three-body terms become negligible.

2.2. Simulation Protocol. The cubic elementary box of 24.6 Å side length contained 1 Ag^+ ion and 499 water molecules corresponding to the density of the system of 0.99702 g/cm^3. A canonical *NVT* ensemble at 298.16 K was used with periodic boundary conditions,[41] and the temperature was kept constant by the Berendsen algorithm.[42] The flexible BJH−CF2 water model[37,43] including an intramolecular potential was used. Consequently, the time step of the simulation was set to 0.2 fs, which allows for explicit movement of hydrogens. A cutoff of 12.0 Å was set except for O−H and H−H non-Coulombic interactions where it was set to 5.0 and 3.0 Å. The reaction field method[44] was used to account for long-range electrostatic interactions.

2.3. QM/MM Molecular Dynamic Simulation. First, a classical simulation was performed for 60 ps. Subsequently, the QM/MM simulation was performed for 16 ps after 4 ps of reequilibration. The ab initio quantum mechanical treatment was applied for the ion and the complete first hydration shell, whereas for the remaining MM region, the same 2+3-body potential as in the classical simulation was used. According to the Ag−O RDF of that simulation, the QM radius had to be set to 3.8 Å in order to fully include the first hydration shell. A smoothing function was applied in the transition region between QM and MM regions. The force of the system, F_{system}, can be defined as

$$F_{system} = F_{MM} + S(F_{QM} - F_{QM/MM}) \quad (5)$$

where F_{MM} is the force of the system derived from the potential function, F_{QM} is the force inside the QM region, calculated by ab initio quantum mechanics, and $F_{QM/MM}$ is the force in the QM region computed using the derivatives of the potential function. S denotes the smoothing function.[45] Free migration of ligands between the QM and MM region is enabled in this approach.

2.4. Velocity Autocorrelation Functions and Mean Residence Times. The evaluation of spectral properties such as librational and vibrational frequencies of water molecule motions is carried out using velocity autocorrelation functions (VACFs), $C(t)$, defined as

$$C(t) = \frac{\sum_{i}^{N_t} \sum_{j}^{N} \vec{v}_j(t_i)\vec{v}_j(t_i + t)}{N_t N \sum_{i}^{N_t} \sum_{j}^{N} \vec{v}_j(t_i)\vec{v}_j(t_i)} \quad (6)$$

where N is the number of particles, N_t is the number of time origins t_i, and $\vec{v}_j$ denotes a certain velocity component of particle j. The power spectrum of the VACF was calculated by Fourier transformation. A correlation length of 2.0 ps was used to obtain the power spectra with 4000 (classical) and 2000 (QM/MM) averaged time origins. Librational and vibrational frequencies

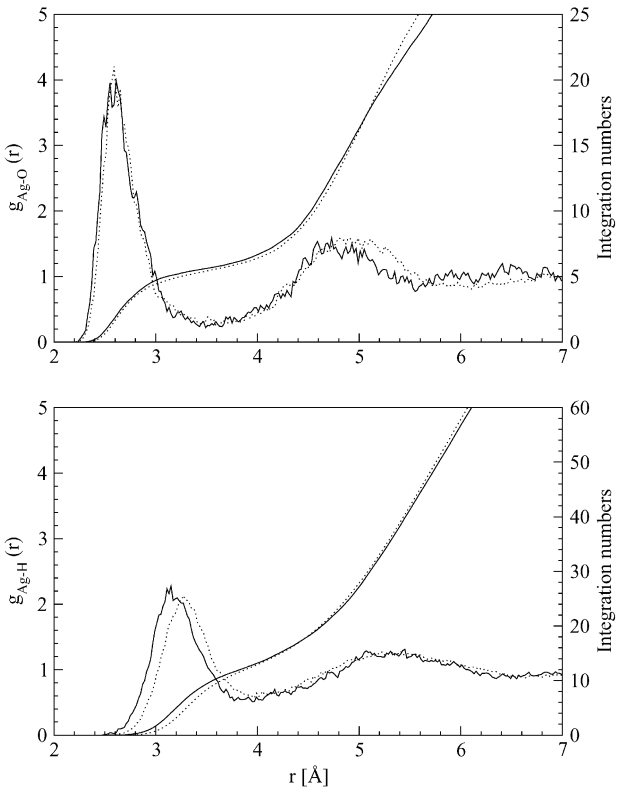

Figure 1. Ag−O and Ag−H radial distribution functions and their corresponding integration numbers obtained from QM/MM (solid line) and classical (dotted line) simulations.

of water molecules as well as ion−oxygen motions were computed using the approximative normal coordinate analysis.[46] Six scalar quantities Q_1, Q_2, Q_3, R_x, R_y, and R_z define the symmetric stretching, bending and asymmetric stretching vibrations, and rotations around the three principal axes of the water molecules.

The mean residence times (τ) of water molecules in the hydration shells of Ag^+ were calculated with the following formalism proposed by Impey et al.[47]

$$n_{\text{ion}}(t) = \frac{1}{N_t}\sum_{n=1}^{N_t}\sum_{j} P_j(t_n, t; t^*) \qquad (7)$$

where $n_{\text{ion}}(t)$ is the number of water molecules which lie initially within the coordination shell and are still there after a time t elapsed. The parameter t^* is introduced to avoid counting of water molecules leaving the coordination shell only temporarily and returning to it within t^*. The function $P_j(t_n,t;t^*)$ of a water molecule j can be either to 0 or 1. It takes the value 1 if molecule j lies within the coordination shell at both time steps t_n and $t + t_n$ and does not leave the coordination shell for any continuous period longer than t^*. Under all other circumstances, it takes the value 0. The parameter of t^* was set to 2 ps in accordance to Impey.[47]

3. Results and Discussion

3.1. Structural Properties. The Ag−O and Ag−H radial distribution functions (RDFs) and their running integration numbers obtained from classical and QM/MM simulations are displayed in Figure 1 and the main structural parameters are listed in Table 2. The maximum probability for the Ag−O and Ag−H distances in the first hydration shell obtained from the QM/MM simulation were observed at ∼2.6 and ∼3.1 Å with a tailed first Ag−O peak (see Figure 1). The broad peak showing some small splitting and shoulders (2.4, 2.49, 2.55, 2.61, 2.7, and 2.81 Å) indicates a very labile structure of the first shell. The value of the Ag−O RDF between first and second hydration shell never comes close to zero, corresponding to frequent intershell water exchange processes and a high flexibility of coordination. The second peak of the Ag−O RDF corresponding to the second hydration shell is well defined and considerably shifted to smaller distances in the QM/MM simulation.

Coordination number distributions of hydrated Ag^+ obtained from classical and QM/MM simulations are displayed in Figure 2, calculated up to a distance of 3.5 Å for the first and 5.5 Å for the second shell. Dominance of 5- and 6-coordinated complexes was obtained from the classical as well as the QM/MM simulation indicating a rather labile structure of the first hydration shell with continuously varying coordination number. In both cases, 7-fold coordinated complexes were also observed which can be seen as transition state structures. Coordination numbers of 5 and 6 are dominant according to both simulations.

TABLE 2: Hydration Parameters for Ag^+ in Aqueous Solution Obtained from QM/MM and Classical Simulations

parameter	classical	QM/MM
r_{1Ag-O}[a]	2.59	∼2.6
r_{2Ag-O}[a]	5.0	4.6
CN 1st[b]	4.9	5.4
CN 2nd[b]	22.6	17.8
O−Ag−O angle	87°	87°
mean out of plane angle[c]	0°	−50°/50°
mean θ angle[d]	158°	135°/145°

[a] First and second peak maximum of Ag−O RDF in Å. [b] Coordination numbers of the first and second hydration shell. [c] Angle between Ag−O connection vector and plane formed by O−H vectors. [d] Angle between Ag−O connection vector and resultant vector from sum of O−H vectors.

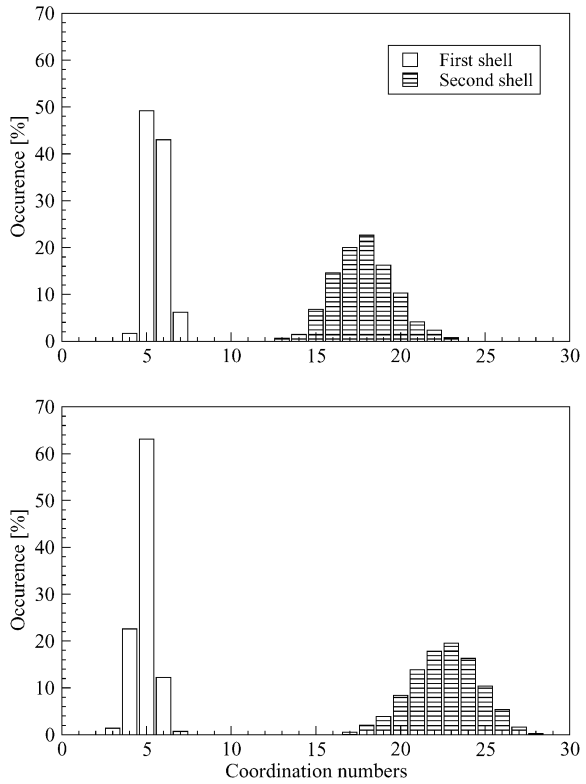

Figure 2. Coordination number distributions of Ag^+ in water obtained from (a) QM/MM and (b) classical simulations.

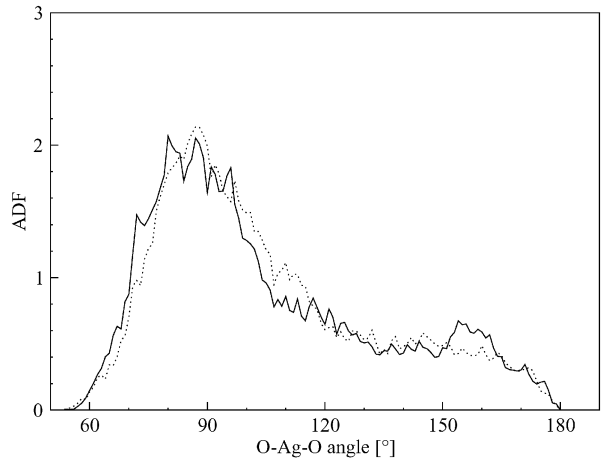

Figure 3. Angular distribution function of $O-Ag^{+}-O$ obtained by QM/MM (solid line) and classical (dotted line) simulations.

Although the Ag−O RDF covers a wide range from 2.2 to 3.5 Å, its average peak value of ∼2.6 Å is quite different from hitherto published experimental distances in the range of 2.3−2.4 Å with an average coordination number of 2−4.5 (cf. Table 3). A possible reason for this discrepancy is the extreme lability and asymmetry of the first hydration shell, which leads to the coexistence of more than one configuration within very short time intervals of a few picoseconds. Experimental data, averaged over a long time and fitted to a single geometrical model configuration instead of a mixture of geometrically very different configurations might thus lead to somewhat different conclusions. A more detailed analysis of our simulation results by visualization tool has been performed, therefore (vide infra). The second shell QM/MM coordination numbers are shifted to considerably lower values in comparison with the classical simulation. The broad distribution and the average value of ∼18 ligands show, however, that this shell is only loosely bound and extremely flexible.

TABLE 3: Structural Parameters of First Hydration Shell of Hydrated Ag^{+}, where *n* Represents the Coordination Number

salt	H_2O/salt molar ratio	r_{Ag-O}, Å	n	geometry	method
Ag^{+}	499	2.59	4.9	irregular	classical MD
Ag^{+}	499	2.6	5.4	irregular	QM/MM MD
Ag^{+}	275	2.3	∼7		MC[a]
$AgClO_4$	16.8	2.31	2.9	irregular	EXAFS[b]
$AgClO_4$	10.4	2.41	2.0	linear	XRD[b]
$AgClO_4$[d]	5555	2.32	4.3	tetrahedral	EXAFS[c]
$AgClO_4$[d]	555	2.31	4.5	tetrahedral	EXAFS[c]
$AgClO_4$[e]	555	2.31	4.3	tetrahedral	EXAFS[c]
$AgClO_4$[e]	10.6	2.41	3.9	tetrahedral	ND[f]

[a] Monte Carlo simulation, ref 7. [b] Experimental values by XRD and EXAFS methods, ref 5. [c] Experimental values by EXAFS method, ref 6. [d] In 0.001 M $HClO_4$. [e] In 3.00 M $HClO_4$. [f] Experimental values by ND method.[49]

The O−Ag−O angle distributions (ADF) of the first shell structure obtained from classical and QM/MM simulations are shown in Figure 3. The peak maxima of the ADFs are ∼87° in both simulations exhibiting a multiply splitted main peak in the QM/MM case again pointing toward the presence of several arrangements. A small second peak located at ∼160° was observed in both simulations, more distinctly in the QM/MM graph.

To illustrate in detail the lability of the first hydration shell with its various configurations, we have created a video clip from the QM/MM simulation trajectory using the MOLVISION

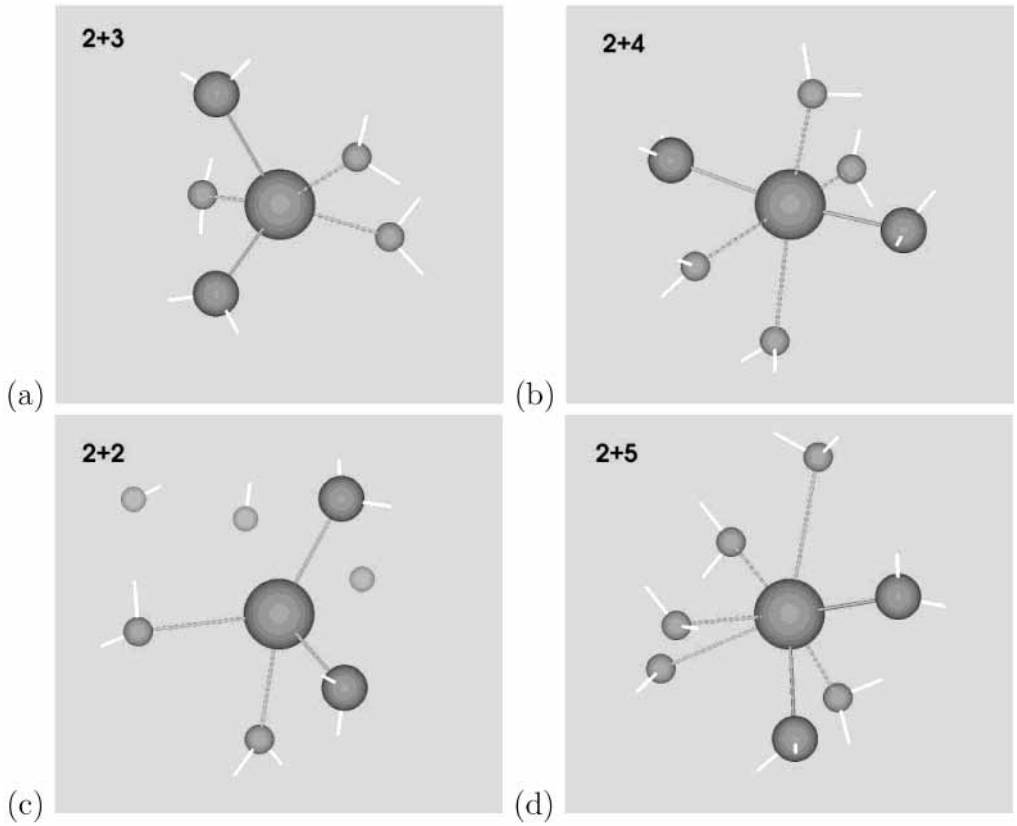

Figure 4. Structures of hydrated Ag^{+} (first shell, using a cutoff of 4.0 Å) showing coordination numbers of (a) 5, (b) 6, (c) 4, and (d) 7. Hydrogen atoms are not shown explicitly, the big sphere represents the Ag^{+} ion, the medium-sized ones are oxygens at distances up to 2.6 Å, and the small ones oxygens at distances above 2.6 Å from the ion (2.6 Å was used due to the slight splitting of the first Ag−O RDF peak).

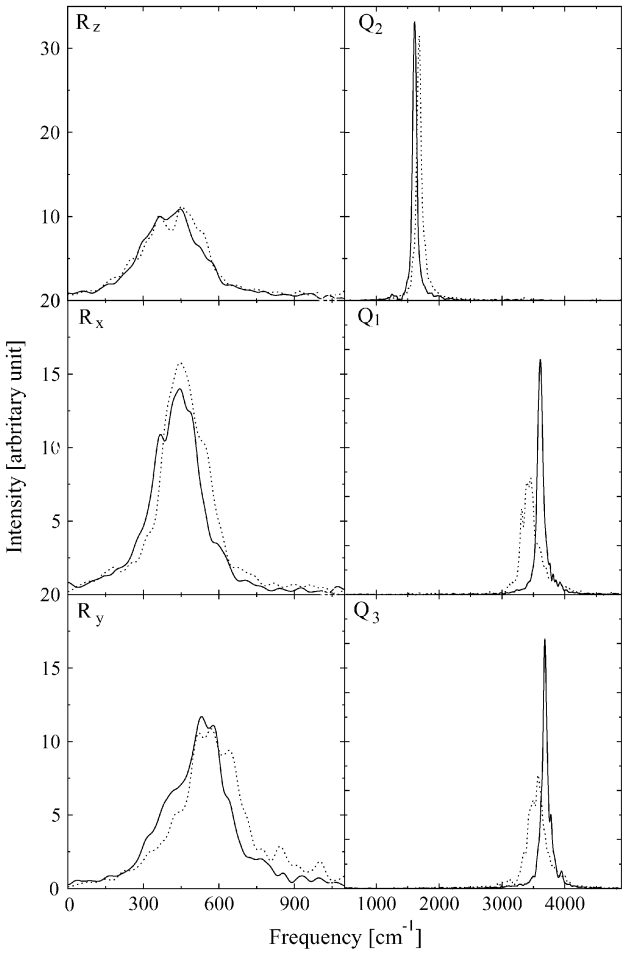

Figure 5. Power spectra of rotational modes R_z, R_x, and R_y and vibrational modes Q_2, Q_1, and Q_3 for water molecules in in the first hydration shell obtained by QM/MM (solid line) and classical (dotted line) simulations.

program and made it available for download at the MOLVISION homepage (http://www.molvision.com, section video clips).[48] The visualization shows a preference of 2+3 and 2+4 configurations in the first hydration shell with two closer and three or four more distant water molecules. The different distances of ligands are consistent with the splittings of the first Ag−O RDF peak. By taking "snapshots" during the simulation, the pictures of 4-, 5-, 6-, and 7-coordinated complexes displayed in Figure 4 were obtained. According to the coordination number distributions, four species configurations exist in the first hydration shell. The dominating ones are the 5- and 6-coordinated complexes (Figure 4, parts a and b), the other structures with 4 and 7 water molecules around the ion (see Figure 5, parts c and d) occur much more rarely (see Figure 2a for percentual occurrence).

Based on the ion-oxygen distances corresponding to the small splittings of the first Ag−O RDF peak one can try to assign more detailed structures, as a 2+3 configuration with 2.5 and 2.7 Å ion−ligand distances and a 2+4 structure with 2.5−2.8 Å. The video clip allows to follow the manifold movements of the ligands including all changes of the coordination number during the simulation. The extreme lability and irregular structure of the solvation shell also corresponds to the splitting of the O/Ag/O angle distribution (Figure 5) and thus supports the above-mentioned reasons for discrepancies with experimental investigations, usually assuming a more or less constant coordination of ligands and reflecting long-time averaged ion-ligand distances.

TABLE 4: Librational and Vibrational Frequencies of Water Molecules in the First and Second Hydration Shell of the Ag^+ Ion and in the Bulk

		frequency [cm^{-1}]					
phase	method	R_z	R_x	R_y	Q_2	Q_1	Q_3
first shell	QM/MM[a]	**447**	**445**	**531**	**1612**	**3610**	**3681**
	classical	452	445	570	1684	3455	3576
second shell	QM/MM	**426**	**466**	**566**	**1689**	**3482**	**3556**
	classical	398	400	575	1693	3441	3542
bulk	QM/MM	**411**	**426**	**551**	**1696**	**3450**	**3550**
	classical	408	420	548	1697	3448	3553
liquid[b]					1645	3345	3445
gas[c]					1595	3657	3756
gas[d]					1601	3641	3756

[a] Using scaled value of 0.89, refs 51 and 52. [b] Experimental values in liquid water, ref 54. [c] Experimental values in gas phase, ref 55. [d] Scaled gas-phase vibrational frequencies using the DZP basis set for water, ref 16.

The hydration energy of Ag^+ resulting from the QM/MM simulation of −152 kcal mol^{-1} is lower than the experimental value of −118 kcal mol^{-1}.[50] The difference may be caused by the specific assumptions necessary to assign single-ion values to measurements of salts[50] and/or by cation/anion associative effects known for silver salts.

The Ag^+ ion has only a small influence on the water geometry in the first shell, leading to 0.01 Å elongation of the O−H bond and a slightly reduced H−O−H angle. The orientation of the ligands is also quite flexible, proving the weak structure-forming ability of Ag^+ even for its nearest environment.

3.2. Librational and Vibrational Motions of Water Molecules. The power spectra of VACFs for the librational motions R_x, R_y, and R_z and the vibrational motions Q_1, Q_2, and Q_3 obtained from classical and QM/MM simulations are displayed in Figure 5 and their frequencies are summarized in Table 4. All frequencies of water molecules and ion−oxygen motions in the first shell obtained by the QM/MM simulation were scaled by the standard factor 0.89,[51,52] because all atomic motions in this shell were generated from the quantum mechanical forces by the analytic gradient of the SCF wave functions. The order $R_z \sim R_x < R_y$ obtained in the first shell of both simulations is in contrast with previous simulations ($R_z < R_x < R_y$).[10,16,53] The frequencies of R_z and R_x values in the first shell from both simulations are blue-shifted in comparison with the bulk by fixation to the ion, whereas a red-shifted R_y frequency value is obtained by the QM/MM simulation. In contrast to this, the classical simulation gives all blue-shifted values. The generally small shifts of R_z, R_x, and R_y values are consistent with the previously deduced labile structure of the first hydration shell, and the observed slight splitting of the corresponding peaks in the QM/MM simulation (cf. Figure 5) confirms the presence of different ion−ligand bonds in different solvate structures. The stretching frequencies of the first hydration shell obtained by the QM/MM simulation are blue-shifted, whereas the bending frequency is red-shifted in comparison to the bulk. The classical simulation gives similar, but much less shifted, values thus showing the significant influence of many-body effects on the vibrational motions. The first shell frequency difference between Q_1 and Q_3 for QM/MM simulation is 71 cm^{-1} which is smaller than in the bulk (100 cm^{-1}).

The power spectra of the Ag^+−O stretching vibration in the first shell obtained by approximative normal coordinate analysis (see section 2.4) from the classical and the QM/MM simulations are displayed in Figure 6. The QM/MM band shows maxima at 99, 142, and 186 cm^{-1} and a shoulder around 245 cm^{-1}. The corresponding force constants are 8, 16, 28, and 48 Nm^{-1}

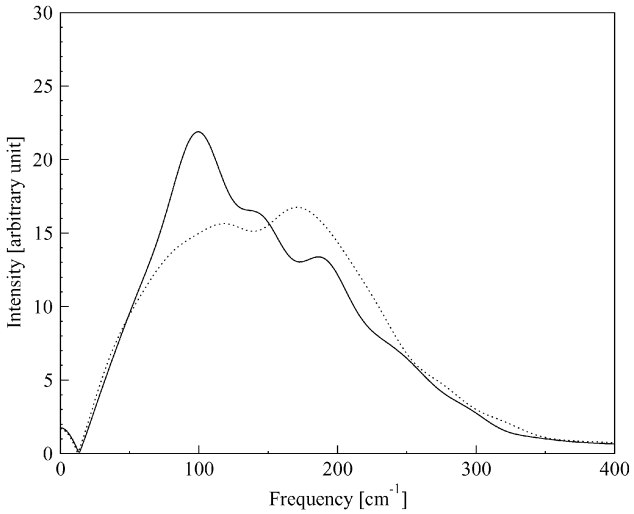

Figure 6. Power spectra of Ag^+−oxygen vibrational modes in the first hydration shell obtained by classical (dotted line) and QM/MM (solid line) simulations.

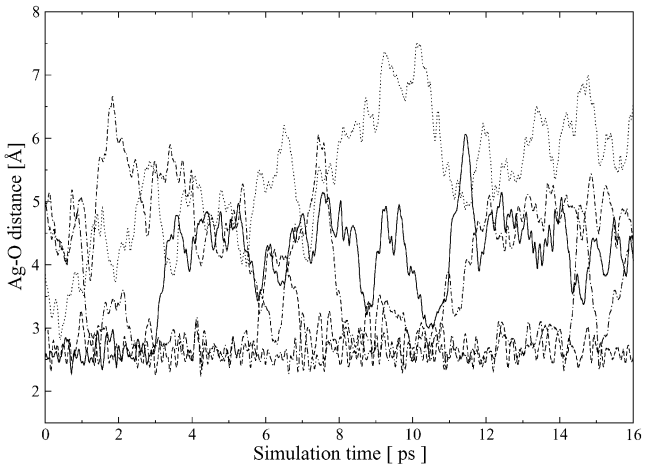

Figure 7. Variation of ion−oxygen distances during the QM/MM simulation showing numerous exchange processes.

(average: ∼25 Nm^{-1}). This variety of values clearly reflect the variety of hydrate structures assumed by the Ag^+ ion, with all different bond lengths and strengths realized in these structures. The "classical" spectrum shows two peaks at 190 and 133 cm^{-1}, proving that even the methodically less accurate simulation does not lead to a single solvate conformation with identical bonds.

3.3. Ligand Exchange Processes. Ion−water distance plots produced during the QM/MM simulation are depicted in Figure 7. Fourteen water molecules have been involved in exchange processes between first and second hydration shell within 16 ps, illustrating the extremely fast dynamics of the first hydration shell and thus its lability.

The mean residence time (MRT) is defined as the average lifetime of a ligand in the coordination shell. The MRT of water molecules in both hydration shells have been calculated from the QM/MM simulation according to section 2.4 with $t^* = 2.0$ ps. The choice of $t^* = 2.0$ ps is rather arbitrary but more or less conventional[47,56] and might be questioned for the case of such fast-exchanging hydration shells. A mean residence time of 25 ps in the first and of 10 ps in the second hydration shell was obtained. If t^* is set to 1.0 ps, the corresponding values are 22 and 6.4 ps.

4. Conclusions

Only QM/MM simulations appear reliable enough to describe in detail the hydration shell structure of Ag^+ as the classical simulation does not reproduce well enough the flexible structural composition of all species formed. Coordination numbers ranging from 4 to 7 have been obtained, showing 5- and 6-fold coordinated complexes to be the dominant species. Vibrational spectra, visualization of dynamics, and the investigation of water exchange processes via mean ligand residence times all lead to a consistent picture of a highly flexible first shell, in which several conformations are interchanging within a picosecond time scale. The presence of geometrically very different species with such short lifetimes can be seen as a reason for difficulties to obtain a precise Ag^+ hydrate structure by experimental methods.

Acknowledgment. Financial support for this work from the Austrian Science Foundation (FWF) (Project P16221-N08) and a scholarship of the Austrian Federal Ministry for Foreign Affairs for R.A. are gratefully acknowledged.

References and Notes

(1) Gabriel, M. M.; Mayo, M. S.; May, L. L.; Simmons, R. B.; Ahearn, D. G. *Curr. Microbiol.* **1996**, *33*, 1.
(2) Nomiya, K.; Takahashi, S.; Noguchi, R.; Nemoto, S. *Inorg. Chem* **1999**, *39*, 3301.
(3) Shoeib, T.; Hopkinson, A. C.; Siu, K. W. M. *J. Phys. Chem. B* **2001**, *105*, 12399.
(4) Boutreau, L.; Léon, E.; Rodríguez-Santiago, L.; Toulhoat, P. *J. Phys. Chem. A* **2002**, *106*, 9359.
(5) Ohtaki, H.; Radnai, T. *Chem. Rev.* **1993**, *93*, 1157.
(6) Seward, T. M.; Henderson, C. M. B.; Charnock, J. M.; Dobson, B. R. *Geochim. Cosmochim. Acta* **1996**, *60* (13), 2273.
(7) Dubois, V.; Archirel, P.; Boutin, *A. J. Phys. Chem. B* **2001**, *105*, 9363−9369.
(8) Loeffler, H. H.; Yagüe, J. I.; Rode, B. M. *Chem. Phys. Lett.* **2002**, *363*, 367.
(9) Loeffler, H. H.; Yagüe, J. I.; Rode, B. M. *J. Phys. Chem. A* **2002**, *106*, 9529.
(10) Tongraar, A.; Liedl, K. R.; Rode, B. M. *J. Phys. Chem. A* **1997**, *101*, 6299.
(11) Tongraar, A.; Rode, B. M. *J. Phys. Chem. A* **1999**, *103*, 8524.
(12) Tongraar, A.; Sagarik, K.; Rode, B. M. *J. Phys. Chem. B* **2001**, *105*, 10559.
(13) Loeffler, H. H.; Rode, B. M. *J. Chem. Phys.* **2002**, *117* (1), 110.
(14) Yagüe, J. I.; Mohammed, A. M.; Loeffler, H. H.; Rode, B. M. *J. Phys. Chem. A* **2001**, *105*, 7646.
(15) Kritayakornupong, C.; Yagüe, J. I.; Rode, B. M. *J. Phys. Chem. A* **2002**, *106*, 10584.
(16) Inada, Y.; Loeffler, H. H.; Rode, B. M. *Chem. Phys. Lett.* **2002**, *358*, 449.
(17) Inada, Y.; Mohammed, A. M.; Loeffler, H. H.; Rode, B. M. *J. Phys. Chem. A* **2002**, *106*, 6783.
(18) Tongraar, A.; Liedl, K. R.; Rode, B. M. *J. Phys. Chem. A* **1998**, *102*, 10340.
(19) Tongraar, A.; Hannongbua, S.; Rode, B. M. *Chem. Phys.* **1997**, *219*, 279.
(20) Tongraar, A.; Liedl, K. R.; Rode, B. M. *Chem. Phys. Lett.* **1998**, *286*, 56.
(21) Schwenk, C. F.; Loeffler, H. H.; Rode, B. M. *Chem. Phys. Lett.* **2001**, *349*, 99.
(22) Schwenk, C. F.; Loeffler, H. H.; Rode, B. M. *J. Chem. Phys.* **2001**, *115* (23), 1080.
(23) Yang, T.; Tsushima, S.; Suzuki, A. *J. Phys. Chem. A* **2001**, *105*, 10439.
(24) Rode, B. M.; Schwenk, C. F.; Tongraar, A. *J. Mol. Liquids* **2002**, in press.
(25) Clementi, E.; Kistenmacher, H.; Kolos, W.; Romano, S. *Theor. Chim. Acta* **1980**, *55*, 257.
(26) Kollman, P. A.; Kuntz, I. D. *J. Am. Chem. Soc.* **1974**, *96*, 4766.
(27) Lybrand, T. P.; Kollman, P. *A. J. Chem. Phys.* **1985**, *83*, 2923.
(28) Curtiss, L. A.; Halley, J. W.; Hautmann, J.; Rahman, A. *J. Chem. Phys.* **1987**, *86*, 2319.
(29) Pranowo, H. D.; Rode, B. M. *J. Phys. Chem. A* **1999**, *103*, 4298.
(30) Marini, G. W.; Liedl, K. R.; Rode, B. M. *J. Phys. Chem. A* **1999**, *103*, 11387.

(31) Marini, G. W.; Texler, N. R.; Rode, B. M. *J. Phys. Chem.* **1996**, *100*, 6808.
(32) Texler, N. R.; Rode, B. M. *J. Phys. Chem.* **1995**, *99*, 15714.
(33) Hay, P. J.; Wadt, W. R. *J. Chem. Phys.* **1985**, *82*, 270.
(34) Dunning, T. R. J. *J. Chem. Phys.* **1970**, *53*, 2823.
(35) Davidson, E. R.; Feller, B. *Chem. Rev.* **1986**, *86*, 681.
(36) Kuchitsu, K.; Morino, T.; Maeda, M. *Bull. Chem. Soc. Jpn.* **1976**, *49*, 701.
(37) Stillinger, F. H.; Rahman, A. *J. Chem. Phys.* **1978**, *98*, 129.
(38) Ahlrichs, R.; Bär, M.; Horn, H.; Häser, M.; Kölmel, C. *Chem. Phys. Lett.* **1989**, *162*, 165.
(39) Ahlrichs, R.; von Arnim, M. *Methods and Techniques in Computational Chemistry: METECC-95*; Cagliari, 1995.
(40) von Arnim, M.; Ahlrichs, R. *J. Comput. Chem.* **1998**, *19*, 1746.
(41) Allen, M. P.; Tildesley, D. J. *Computer Simulation of Liquids*; Oxford University Press: New York, 1987.
(42) Berendsen, H. J.; Grigera, J. R.; Straatsma, T. P. *J. Phys. Chem.* **1983**, *91*, 6269.
(43) Bopp, P.; Janscó, G.; Heinzinger, K. *Chem. Phys. Lett.* **1983**, *98*, 129.
(44) Adams, D. J.; Adams, E. M.; Hills, G. J. *J. Mol. Phys.* **1985**, *38*, 387.
(45) Markham, G. D.; Bock, J. P. G. C. L.; Trachtman, M.; Bock, C. W. *J. Phys. Chem.* **1996**, *100*, 3488.
(46) Bopp, P. *Chem. Phys.* **1986**, *106*, 205.
(47) Impey, R. W.; Maden, P. A.; McDonald, I. R. *J. Phys. Chem.* **1983**, *87*, 5071.
(48) Tran, H. T.; Rode, B. M. www.molvision.com, 2002.
(49) Sandström, M.; Neilson, G. W.; Johansson, G.; Yamaguchi, T. *J. Phys. C: Solid State Phys.* **1985**.
(50) Marcus, Y. *J. Chem. Soc., Faraday Trans. 1* **1987**, *83*, 339.
(51) Scott, A. P.; Radom, L. *J. Phys. Chem.* **1996**, *100*, 16502.
(52) DeFrees, D. J.; McLean, A. D. *J. Chem. Phys.* **1985**, *82* (1), 333.
(53) Schwenk, C. F.; Loeffler, H. H.; Rode, B. M. *J. Am. Chem. Soc.* **2003**, *125*, 1618−1624.
(54) Murphy, W. F.; Bernstein, H. *J. J. Phys. Chem.* **1972**, *76*, 1147.
(55) Eisenberg, D.; Kauzmann, W. *The Structure and Properties of Water*; Oxford University Press: Oxford, U.K., 1969.
(56) García, A. E.; Stiller, L. *J. Comput. Chem.* **1993**, *14* (11), 1396.